Optical properties of nondegenerate ground-state polymers: Three dioxythiophene-based conjugated polymers

J. Hwang and D. B. Tanner
Department of Physics, University of Florida, Gainesville, Florida 32611

I. Schwendeman and J. R. Reynolds
Department of Chemistry, University of Florida, Gainesville, Florida 32611

(Received 16 June 2002; revised manuscript received 26 November 2002; published 18 March 2003)

We report the optical properties of three dioxythiophene-based conjugated polymers: poly(3,4-ethylenedioxythiophene) poly(3,4-propylenedioxythiophene), and poly(3,4-(2,2-dimethylpropylenedioxy)-thiophene). Films of ca. 200 nm thickness of these polymers were prepared on indium-tin-oxide coated glass substrates using a potentiostatic electropolymerization method. The reflectance and transmittance of the samples were measured over a broad energy range from the midinfrared through the ultraviolet. To extract the optical constants of the polymers, we modeled all of the layers of this multilayer thin-film structure using a Drude-Lorentz model. From the parameters obtained, we compute the optical constants, such as absorption coefficient and frequency-dependent conductivity. These functions yield information about the electronic structure of the neutral and doped polymers, which show evidence for polaron states at low doping and bipolarons at the maximum doping level. We observed doping-dependent changes in the electronic structure of these polymers as well as doping-induced infrared-active vibrational modes.

DOI: 10.1103/PhysRevB.67.115205 PACS number(s): 76.50.+g, 75.50.Ee

I. INTRODUCTION

High levels of electronic conductivity are accessible in π-conjugated polymers in their redox doped (oxidized or reduced) forms. Ever since the initial discovery of this effect,[1] conjugated polymers have been studied intensively on account of this high conductivity, reversible doping, and low-dimensional geometry. Typically, conjugated polymers are classified into two groups: degenerate ground-state polymers[2–4] and nondegenerate ground-state polymers.[2,4–7]

In examining and comparing these two polymer types, degenerate ground-state polymers are the simpler to model. In these polymers, interchange of single and double bonds on the polymer backbone produces a conjugated chain with identical electronic structure, and gives rise to the possibility of solitonic defects. In nondegenerate ground-state polymers, the interchange of single and double bonds along the polymer backbone yields two states of different energies; i.e., there is no degeneracy in the ground-state energy for the single-double bond interchange transformation, leading to polaron or bipolaron states for charged defects on the polymer. Quantum-chemical calculations of the electronic structure of the polaron and bipolaron have been done on specific nondegenerate ground-state polymers [e.g., poly(*p*-phenylene), polypyrrole, and polythiophene].[4,5]

There are important experimental signatures of polaron or bipolaron formation in nondegenerate ground-state polymer systems: (1) infrared-active vibrational (IRAV) modes in the midinfrared attributable to structural distortions, (2) midgap states and associated electronic transitions (polaronic or bipolaronic), which are revealed by optical-absorption experiments.

Figure 1 shows the general features of the doping-induced electronic structure and the corresponding optical-absorption bands of nondegenerate ground-state polymers; the polaron is the expected state when the system is lightly doped, whereas the bipolaron is the expected state when the system is heavily doped. Polarons and bipolarons exhibit different absorption spectra: the polaron state yields three broad peaks, whereas the bipolaron state yields only a single, even broader, peak.

In this paper, we study the optical properties of three nondegenerate ground-state polymers belonging to the dioxythiophene family: poly(3,4-ethylenedioxythiophene) (PEDOT), poly(3,4-propylenedioxythiophene) (PProDOT), and poly(3,4-(2,2-dimethylpropylenedioxy)thiophene) (PProDOT-Me_2). The relevance for the study and comparison of these optoelectronic polymers is evident, as they have already proved to be useful for several smart window applications.[9] Moreover, a recent study shows that these materials are able to modulate the reflectivity of a metal surface over a broad range of the electromagnetic spectrum, including the visible, the near infrared, and the midinfrared.[10] Here, we present reflectance and transmittance data for the above polymers deposited as thin films on indium-tin-oxide (ITO)/glass substrates, along with a discussion of the doping-induced electronic structure and the infrared-active vibrational modes as a function of a redox state.

II. EXPERIMENT

A. Sample preparation

Figure 2 shows chemical structures of the polymer repeat units. This group of conjugated polymers has high stability in air and at high temperatures ($\sim$120 °C) in their doped states.[13] EDOT was received as a gift from Bayer A.G. whereas ProDOT and ProDOT-Me_2 were synthesized using a published procedure.[11,12] Oxidative electrochemical polymerization is the most direct method to deposit polymer

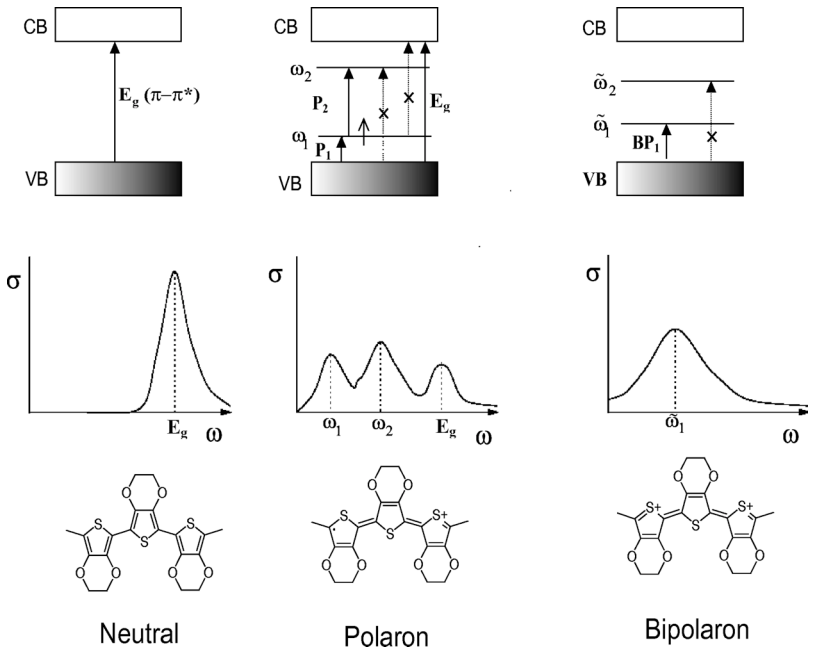

FIG. 1. Electronic structure of polarons and bipolarons in nondegenerate ground-state polymers. Vertical lines show the electronic transitions. The lines with × are for transitions that are not allowed because of symmetry or the dipole selection rule (Ref. 8). $P_1=\omega_1$, $P_2=\omega_2-\omega_1$, and $BP_1=\tilde{\omega}_1$. (Here BP means bipolaron.) The small arrow stands for an electron with a spin (either up or down).

films on ITO/glass working electrodes. We employed a conventional three-electrode electrochemical cell with a Pt flag counter electrode. For control of the electrochemical potential, an Ag/Ag^+ reference was placed between the working electrode and the counter electrode. All three electrodes were connected to an EG&G PAR model 273A potentiostat/galvanostat, which allowed us to monitor the charge passed as a function of time. Our films were prepared from a 10-mM monomer in tetrabutylammonium perchlorate/acetonitrile solutions. We applied 1.0 V vs Ag/Ag^+ for EDOT polymerization and 1.1 V vs Ag/Ag^+ for both PProDOT and PProDOT-Me_2.

The polymerization proceeds with the oxidation of the heterocyclic monomer at the working electrode immediately followed by a chemical coupling of two radical cations to give a dication dimer, which loses two protons, yielding the neutral dimer. Subsequent oxidations and couplings yield conducting oligomers in the vicinity of the electrode. Once these oligomers reach a length at which they become insoluble in the electrolyte solution, they electroprecipitate onto the working electrode surface. Because oxidation of the monomer occurs at a higher potential than that of the polymer, the electroactive film is deposited in its doped state, containing ClO_4^- ions. Experiments done in our group suggest that the doping level corresponds to one ClO_4^- dopant ion for every three or four rings. Typical film thicknesses, measured utilizing a Dektak Sloan 3030 profilometer, were in the range of 200 nm. The optical fitting procedure, described below, also produces estimates of thickness in this range.

Lowering the potential after electrosynthesis results in the reduction of the polymer film from the oxidized to neutral state. The electrochemical reduction used a potential of -1.0 V vs Ag/Ag^+, applied for about 10 min. It was followed by a further chemical reduction by treatment with a solution of 85% by weight of hydrazine in water for a period of 5 min to ensure that all the dopant ions (ClO_4^- in this case) were removed from the film and the polymer was fully charge neutralized.

The polymers in the reduced state are oxygen sensitive, due to their electron-rich character. Consequently, the neutral films exposed to air become lightly *p* doped in less than 1 min, the doping level reaching a saturation value over several hours. To obtain fully neutral samples, the electrochemical as well as the chemical reduction processes were carried out in an Ar-filled glove bag (AtmosBag from the Aldrich Chemical Co). Subsequently, we installed the neutral polymer sample in a sealed optical sample cell in the glove bag. The cell used KCl windows, transparent over the midinfrared through the ultraviolet region. and was filled with Ar for the reflectance and transmittance measurements. In all these procedures, we handled the neutral polymer films under Ar to avoid exposure to oxygen and moisture.

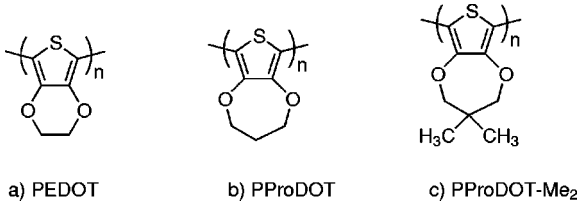

FIG. 2. Chemical structures of (a) PEDOT, (b) PProDOT, and (c) PProDOT-Me_2.

B. Optical measurements

All samples consisted of three layers: thick glass substrate (~0.67 mm), thin ITO layer (~250 nm), and thin polymer layer (~200 nm). The aerial dimension of the sample is 0.7×0.5 cm^2. We used three spectrometers for our optical measurements: a Bruker 113v Fourier-transform infrared spectrometer (400–5000 cm^{-1}), a Zeiss MPM 800 microscope photometer (4500–45 000 cm^{-1}), and a modified

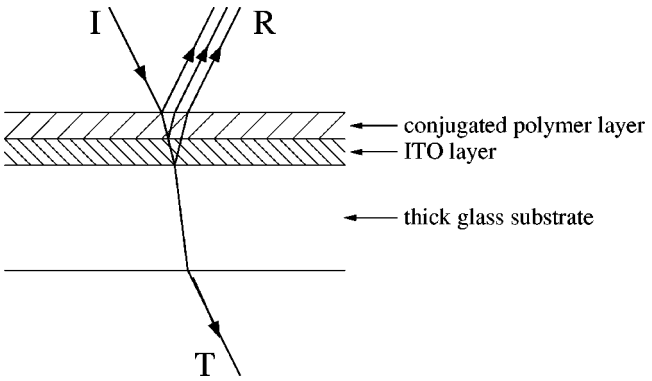

FIG. 3. Cross section of a polymer film on ITO/glass slide.

Perkin-Elmer 16U (3700–45 000 cm^{-1}). All measurements were performed at room temperature (300 K). We measured the reflectance and the transmittance of all three polymers for their three different phases. Because we used an aluminum (Al) mirror as a reference for reflectance measurements, we corrected the measured reflectance data for the known reflectance of Al.

III. RESULTS AND DISCUSSION

A. Reflectance and transmittance spectra

The samples studied consisted of a thin polymer layer on an ITO layer on a thick glass substrate (polymer/ITO/glass), shown schematically in Fig. 3. Light incident on the polymer surface reflects from all three layers; the absorption within each layer as well as the reflection from each interface contributes to the measured reflectance and transmittance spectra. Multiple internal reflections within the polymer, the ITO layers, and the glass substrate (not shown in the diagram) also contribute. We estimated the optical constants of the polymers by using fits to model dielectric functions for a multilayer film; Sec. IV presents the results of this analysis.

The reflectance and transmittance spectra for three different states (neutral, lightly doped, fully doped) of three polymers (PEDOT, PProDOT, and PProDOT-Me_2) are shown in Figs. 4–6, respectively, along with fits to the multilayer Drude-Lorentz model (discussed below). All three layers contribute to these spectra, with the electrochromic polymer contribution most evident in the visible-region transmittance spectra. As is known from spectroelectrochemistry,[14] the neutral state shows a strong optical transition at about 2.5 eV (20 000 cm^{-1}), due to the π-π^* transition of the undoped polymer. This feature is seen in our transmittance data as a deep minimum at this energy. As the polymer is doped, this feature becomes weaker, and is absent in the spectra of the fully doped polymer.

In the infrared region the spectrum is affected by all three materials in the sample. The glass and the ITO film prevent any transmission at energies lower than 0.3 eV (2500 cm^{-1}); the ITO has high reflectance at energies lower than about 0.4 eV (3000 cm^{-1}), especially in the insulating (undoped) phase where the polymer is highly transparent; the infrared-active vibrational modes of the polymer are evident

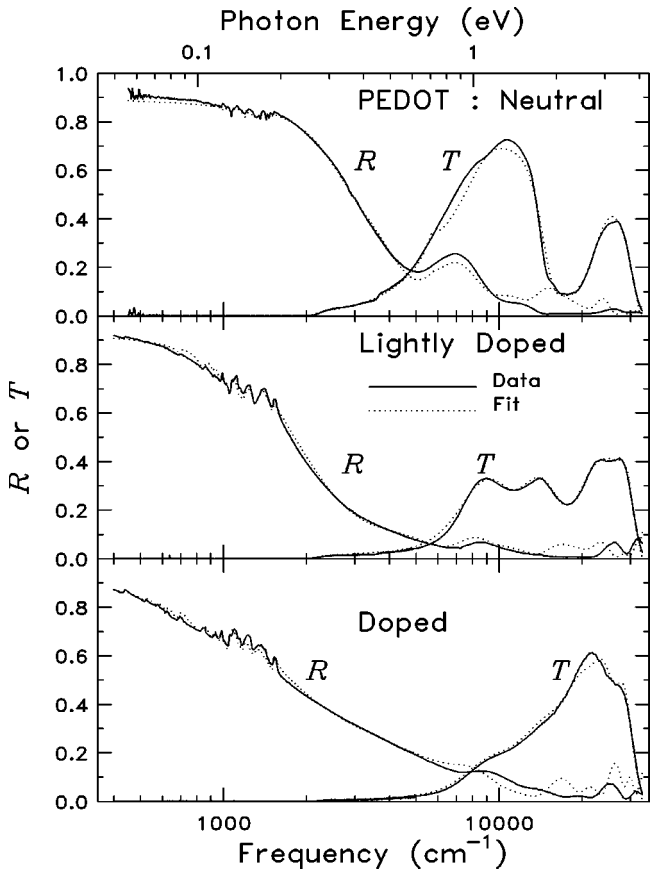

FIG. 4. Reflectance and transmittance of neutral, lightly doped, and fully doped states of PEDOT, data and fits.

between 800 and 1600 cm^{-1}. Note that new, strong vibrational features appear in the doped state.

Even though the fully doped polymers have relatively high dc conductivity values (above 100 S/cm), the midinfrared reflectance is actually smaller in the doped state than in the neutral state. This behavior is a consequence of the fact that the ITO layer is more conducting than the doped polymers. The midinfrared reflectance of the neutral sample is dominated by the polymer/ITO interface, and this reflectance is larger than the reflectance of the vacuum/polymer interface in the doped sample.

B. Analysis: Thin film optics and Drude-Lorentz model

We have used thin-film optics and the Drude-Lorentz model to model the optical properties of the multilayer samples. The thin-film optics problem[15] begins with a single layer of thickness d_1 and complex index of refraction $\tilde{n}_1$ located between two semi-infinite media with indices of refraction $\tilde{n}_0$ and $\tilde{n}_2$. Although the light experiences multiple reflections within the thin layer, one may use the resultant electric-field vectors and match boundary conditions at the two interfaces. This approach yields a matrix equation:

$$\begin{pmatrix} 1 \\ \tilde{n}_0 \end{pmatrix} + \begin{pmatrix} 1 \\ -\tilde{n}_0 \end{pmatrix} r_1 = M_1 \begin{pmatrix} 1 \\ \tilde{n}_2 \end{pmatrix} t_1 \qquad (1)$$

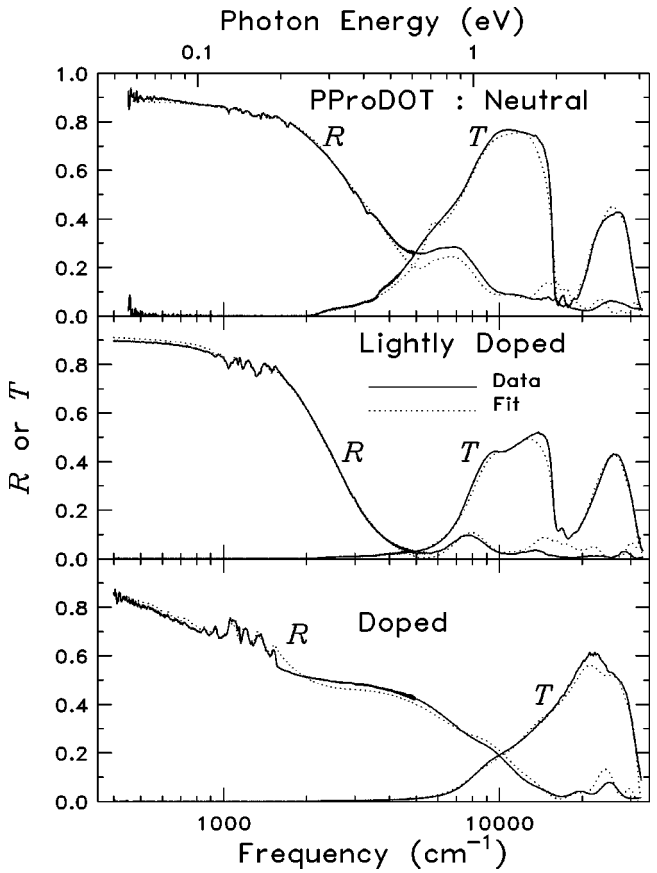

FIG. 5. Reflectance and transmittance of neutral, lightly doped, and fully doped states of PProDOT, data and fits.

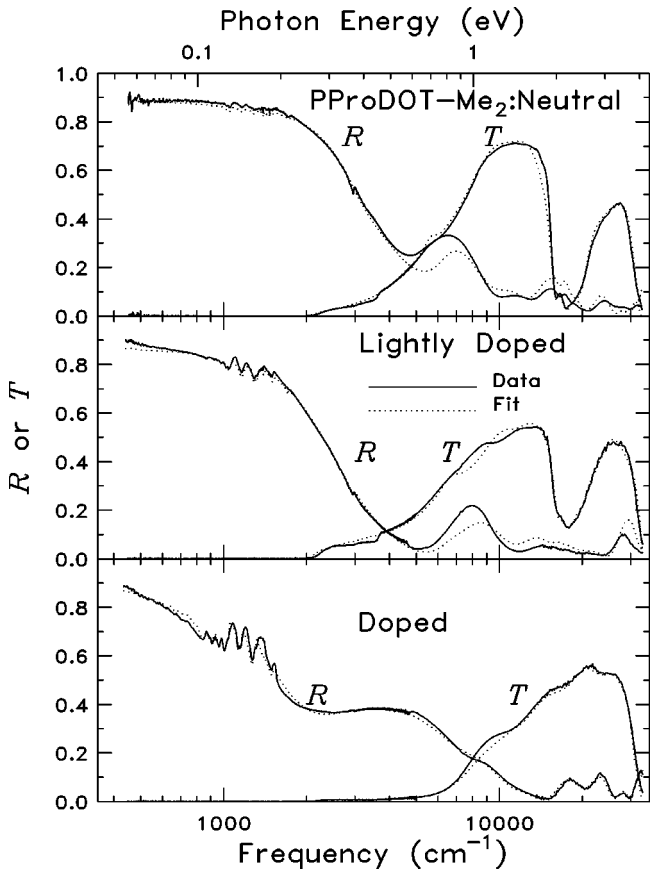

FIG. 6. Reflectance and transmittance of neutral, lightly doped, and fully doped states of PProDOT-Me$_2$, data and fits.

where we have assumed unit amplitude for the incident electric-field vector. The coefficient r_1 is then the amplitude of the reflected resultant electric-field vector at the first interface, and t_1 is the amplitude of the resultant transmitted field behind the second interface. The quantity M_1 is known as the transfer matrix of the single layer; it is given by

$$M_1 \equiv \begin{pmatrix} \cos\delta_1 & -\frac{i}{\tilde{n}_1}\sin\delta_1 \\ -i\tilde{n}_1\sin\delta_1 & \cos\delta_1 \end{pmatrix}. \tag{2}$$

This matrix contains all the information about a single layer: the complex index of refraction and the thickness of the layer are contained in $\delta_1=(2\pi/\lambda)\tilde{n}_1 d_1\cos\theta$. (For normal incidence $\theta=0$.) If we solve the matrix equation for r_1 and t_1, we obtain the reflectance and transmittance of the layer:

$$\mathcal{R}_1 \equiv r_1(r_1)^*, \quad \mathcal{T}_1 \equiv \frac{\tilde{n}_2}{\tilde{n}_0} t_1(t_1)^*. \tag{3}$$

Knowing $\tilde{n}_1$ and thickness d, we can compute the reflectance and transmittance of the film.

This approach extends in a straightforward way to an N-layer system.[15] Each transfer matrix carries information for one layer, and the resultant transfer matrix M_N is simply the product of all transfer matrices for the N layers, i.e., $M_N=M_1M_2\cdots M_n$, where M_n is the transfer matrix of the nth layer. Replacing M_1 with M_N in Eq. (1), allows the calculation of the reflectance and transmittance of the N-layer system, assuming that one knows all the $\tilde{n}_i \equiv \sqrt{\tilde{\epsilon}_i}$, where $\tilde{\epsilon}_1$ is the complex dielectric function of layer i.

The Drude-Lorentz model[16] used for the complex dielectric function of each layer may be written

$$\tilde{\epsilon}(\omega) = \epsilon_\infty - \frac{\omega_{pD}^2}{\omega(\omega+i/\tau)} + \sum_j \frac{\omega_{pj}^2}{\omega_j^2-\omega^2-i\omega\gamma_j}. \tag{4}$$

The first term ϵ_∞ is the limiting high-frequency behavior of $\epsilon(\omega)$. The second (Drude) term represents the free carrier (metallic) contribution, in which $\omega_{pD}(\equiv\sqrt{4\pi ne^2/m^*})$ is the Drude plasma frequency (with m^* being the effective mass of the free carriers) and τ is the relaxation time associated with collisions between free carriers and impurities, phonons, or other excitations in the metal. The final sum, the Lorentz dielectric function, does double duty and is able to represent both the contributions of bound carriers and the contributions of phonons. Here the quantities ω_j, γ_j, and ω_{pj}, $(\equiv\sqrt{4\pi n_j e^2/m_j^*})$ are, respectively, the resonant frequency, damping constant, and plasma frequency or oscillator strength of the jth Lorentz absorption band.

Our procedure consists of fitting the measured reflectance and transmittance using the Drude-Lorentz model for each of

TABLE I. The fitting parameters for neutral, slightly doped, and doped PEDOT. Here, d is the thickness of the film.

Neutral			Slightly doped			Doped		
ω_{pj} (cm^{-1})	ω_j (cm^{-1})	γ_j (cm^{-1})	ω_{pj} (cm^{-1})	ω_j (cm^{-1})	γ_j (cm^{-1})	ω_{pj} (cm^{-1})	ω_j (cm^{-1})	γ_j (cm^{-1})
						866	0	809
2000	3000	2300	8500	2925	6691	12380	1098	9192
7350	15870	3000	4600	4500	4500	8267	3467	9105
4950	17200	3000	5300	11300	4700	4120	11459	7500
4790	18500	3000	7757	17556	6711	26117	39342	1525
6429	20501	4855	3209	20966	8265			
8769	31050	8860	2672	26305	5727			
			13294	43540	28396			
100	852	20	300	685	37	210	515	15
90	918	10	430	845	50	200	570	18
50	955	8	180	917	20	270	620	20
130	985	18	110	935	14	500	684	35
65	1030	10	300	975	30	600	790	100
220	1070	17	200	1018	35	570	835	50
50	1090	8	470	1059	35	600	915	45
230	1197	50	100	1085	14	450	970	26
35	1263	5	140	1140	25	120	1007	10
380	1305	55	550	1187	80	750	1047	43
320	1320	80	350	1335	80	200	1070	13
110	1360	10	70	1360	20	150	1135	17
100	1430	10	50	1380	20	520	1180	50
110	1462	15	120	1490	20	300	1190	70
45	1496	10	220	1510	40	640	1300	80
90	1510	25				100	1360	15
						90	1410	10
						150	1480	20
						420	1515	40
$\epsilon_\infty =$	1.90		$\epsilon_\infty =$	1.98		$\epsilon_\infty =$	2.17	
$d =$	210 nm		$d =$	211 nm		$d =$	225 nm	

the three layers in our polymer/ITO/glass samples, adjusting the parameters (including the layer thickness) for a best fit to *both* measured quantities. To simplify the task of obtaining results for the polymer/ITO/glass samples, we measured the reflectance and transmittance of bare glass and of the ITO/glass samples without polymer. The analysis of these measurements gave the Drude-Lorentz model parameters for the glass and for the ITO layer. Then, when we fitted the measured transmittance and reflectance data for the polymer/ITO/glass samples, we used the already-obtained parameters for the ITO layer and the glass substrate. In each case, the thickness of the layer was considered to be an adjustable parameter.

The Drude-Lorentz model fits are shown as dotted lines in Figs. 4–6. The parameters used to fit the data are shown in Tables I–III. Note that for each of the nine samples studied, the reflectance and the transmittance were fitted with a single set of parameters. There are four blocks of data in the tables, which correspond, respectively, to the free-carrier (Drude) conductivity (significant only in the doped films), electronic transitions, phonons, and ϵ_∞ and thickness. It required several oscillators to fit many of the bands in Figs. 4–6. For example, the π-π^* transition in the visible was fit with between 3 and 5 distinct Lorentz oscillators. There are two reasons why we required so many parameters. First, the bands have vibronic structure, requiring one oscillator for each of the 2 or 3 sidebands evident in the spectra. Second, we used in some cases two closely spaced and overlapping oscillators in order to try to fit the steeply rising absorption edges of this band.

Generally speaking, the fit produced excellent results in the midinfrared, but deviated from the experimental results in the near infrared and visible. This is despite the fact that the least-squares program[17] returned χ^2 values below 3×10^{-4}. We believe that there are two causes of these difficulties. One is the steepness of the absorption edge of the π-π^* transition mentioned above. Second, much of the structure in the near infrared through visible region, particularly in the reflectance spectra, is attributable to multiple internal reflections within the thin films, and our assumption of

TABLE II. The fitting parameters for neutral, slightly doped, and doped PProDOT. Here, d is the thickness of the film.

Neutral			Slightly doped			Doped		
ω_{pj} (cm^{-1})	ω_j (cm^{-1})	γ_j (cm^{-1})	ω_{pj} (cm^{-1})	ω_j (cm^{-1})	γ_j (cm^{-1})	ω_{pj} (cm^{-1})	ω_j (cm^{-1})	γ_j (cm^{-1})
						1,042	0	511
1598	2901	3233	7108	4303	7755	15500	938	9200
1602	3114	2347	2400	10881	4000	8200	3005	3819
5200	16300	900	3400	16200	1100	3864	28573	4176
6500	17600	1450	5200	17700	2300			
3300	18900	1100	6200	19500	4468			
5000	20173	2500	8937	30175	21398			
3332	22702	3776						
10241	32202	14474						
100	930	40	110	862	30	250	525	30
210	1047	25	250	932	50	400	620	20
50	1080	10	75	980	20	500	669	27
100	1135	15	50	1010	8	600	715	35
170	1180	30	430	1047	55	900	780	100
270	1280	80	140	1080	17	700	837	50
110	1320	30	150	1130	20	750	895	50
140	1367	20	340	1180	45	500	920	40
50	1411	15	60	1210	10	1100	990	65
100	1435	15	90	1265	10	350	1012	20
70	1470	10	90	1285	20	900	1040	35
160	1500	50	400	1325	70	170	1075	10
40	1525	8	140	1362	24	500	1090	50
120	1645	100	70	1385	15	240	1131	10
110	1700	45	30	1410	10	750	1170	30
145	1712	45	60	1430	10	500	1190	50
			55	1470	10	450	1262	25
			165	1500	30	400	1290	20
			30	1520	8	600	1310	60
			100	1710	80	250	1355	20
						140	1380	20
						300	1430	60
						700	1500	50
$\epsilon_\infty =$	1.98		$\epsilon_\infty =$	1.73		$\epsilon_\infty =$	2.15	
$d =$	212 nm		$d =$	246 nm		$d =$	175 nm	

a layer of uniform thickness (i.e., with parallel faces) is probably oversimplified. We obtained better fits to the transmittance spectra than to the reflectance spectra in this wavelength region.

IV. OPTICAL CONSTANTS AND DISCUSSION

We can compute any of the optical ''constants'' of our materials by using the parameters from the Drude-Lorentz fit. These parameters consisted of three quantities for each absorption band (center frequency, width, and spectral weight), ϵ_∞, and thickness. The optical conductivities and absorption coefficients for PEDOT, PProDOT, and PProDOT-Me_2 are shown in Figs. 7 and 8, respectively.

In these results (which we stress are the results from the fit of our model dielectric function to reflectance and transmittance and are not derived from the Kramers-Kronig analysis or from inversion of the reflectance and transmittance data) the properties of the polymers in their neutral, lightly doped, and fully doped states are much clearer than in the reflectance or transmittance spectra. The neutral polymers have low conductivity in the infrared (except for the vibrational structure) and a first optical transition in the visible region, with the maximum conductivity occurring at 2.14 eV (PEDOT), 2.03 eV (PProDOT), and 2.17 eV (PProDOT-Me_2). In the lightly doped samples, this intense absorption is reduced by about a factor of 2 in spectral weight, and two new bands appear at about 0.62 and 1.4 eV. (These bands are most evident in PEDOT, but occur in all three lightly doped samples.) The doped polymers exhibit a

TABLE III. The fitting parameters for neutral, slightly doped, and doped PProDOT-Me_2. Here, d is the thickness of the film.

Neutral			Slightly doped			Doped		
ω_{pj} (cm^{-1})	ω_j (cm^{-1})	γ_j (cm^{-1})	ω_{pj} (cm^{-1})	ω_j (cm^{-1})	γ_j (cm^{-1})	ω_{pj} (cm^{-1})	ω_j (cm^{-1})	γ_j (cm^{-1})
						1042	0	865
1700	3354	2000	5070	3751	5569	10923	1255	8999
1000	5672	1777	2450	11434	3500	10304	3264	4160
5200	16000	1000	2622	16300	1144	2568	12336	4000
6800	17382	1400	6767	17700	3366	3442	21869	13580
7800	19001	3244	2161	19822	1686	8964	33464	24511
8605	26217	17133	5573	21946	7018			
2859	31918	3415	3621	31787	14164			
120	915	45	150	872	30	200	530	20
125	1027	20	85	925	10	200	580	20
205	1055	25	70	950	10	300	623	20
45	1130	8	130	980	20	250	667	20
230	1170	45	170	1023	20	500	710	60
80	1233	27	300	1052	30	250	780	25
40	1260	8	400	1170	50	800	855	55
80	1287	25	50	1190	8	100	890	7
200	1292	60	340	1300	45	700	918	40
45	1317	12	70	1315	10	580	970	30
50	1330	10	170	1331	16	1000	1025	50
70	1362	12	65	1360	10	500	1050	20
110	1395	10	80	1395	8	420	1140	25
120	1435	25	70	1435	20	590	1163	25
98	1470	10	60	1470	10	750	1285	40
80	1510	20	180	1505	35	200	1313	10
120	1720	45	150	1710	100	80	1350	7
						80	1380	8
						80	1400	8
						400	1510	40
$\epsilon_\infty =$	2.19		$\epsilon_\infty =$	2.27		$\epsilon_\infty =$	2.43	
$d =$	198 nm		$d =$	239 nm		$d =$	190 nm	

single broad band, with a maximum at about 0.71 eV. The vibrational structure is considerably enhanced in the doped samples, as will be discussed below.

By extrapolation of the low-frequency conductivities (Fig. 7) to zero frequency, we estimate the dc conductivities of the three polymers in their doped states to be 250 S/cm for doped PEDOT, 390 S/cm for doped PProDOT, and 150 S/cm for doped PProDOT-Me_2. Although these values are extrapolations from rather high infrared frequencies, they suggest that doped PProDOT has the highest dc conductivity.

A. Doping-induced electronic structure

The electronic structure of the polymers may be discussed in terms of either the optical conductivity or the absorption coefficient. These quantities are closely related, because $\alpha = 4\pi\sigma_1/nc$ where α is the absorption coefficient, σ_1 is the conductivity, n is the real index of refraction, and c is the speed of light. The absorption coefficients (Fig. 8), display broad electronic absorption bands (some with clear vibronic structure) and narrow vibrational absorption bands.

The π-π^* transition is the primary electronic transition in the neutral polymer. As the polymers are converted from the neutral state to the lightly doped state, there is a blueshift in the π-π^* transition energy because the new doped states are created from the top of the π band. In the case of PEDOT, this blueshift is about 450 cm^{-1}; for PProDOT, 250 cm^{-1}; and for PProDOT-Me_2, 350 cm^{-1}. Moreover, the intensities of the π-π^* transitions for the all three polymers decrease and finally disappear as the doping level increases.

The π-π^* transitions of the neutral PProDOT and PProDOT-Me_2 show clear vibronic splitting, identified by several sharp peaks within the π-π^* transition. These features are observed when the equilibrium geometries of the ground and excited electronic states differ. For PProDOT, the lowest two maxima are at 16 400 cm^{-1} and 17 750 cm^{-1}. For PProDOT-Me_2, we find peaks at 16 150 cm^{-1} and at 17 500 cm^{-1}. In both PProDOT and PProDOT-Me_2 the vi-

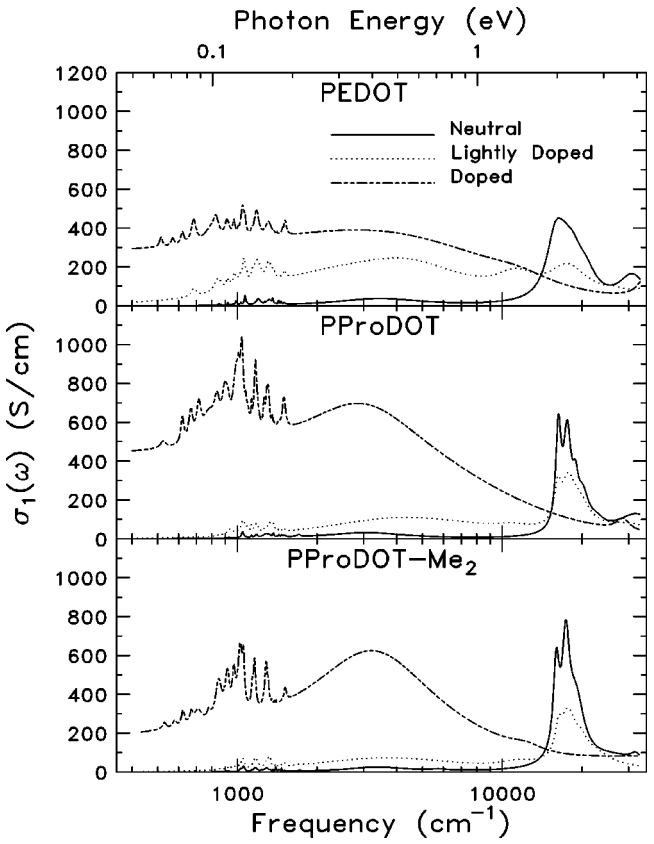

FIG. 7. The optical conductivities of PEDOT, PProDOT, and PProDOT-Me_2.

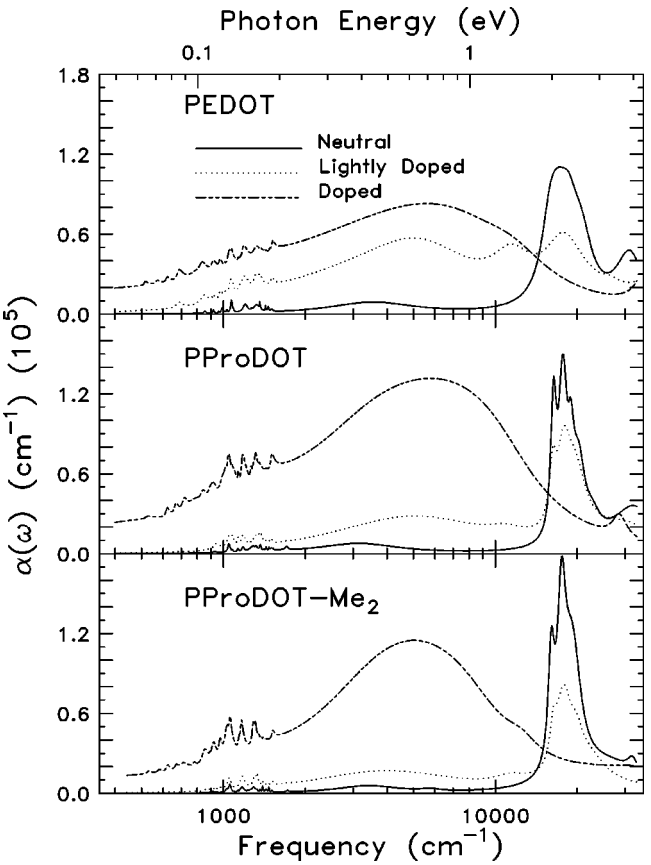

FIG. 8. The absorption coefficients of PEDOT, PProDOT, and PProDOT-Me_2.

bronic splitting is 1 350 cm^{-1}, suggesting that the same vibration, probably a C-C stretching frequency, couples to the electronic coordinates. The origin of the difference between the ground and excited states implies a high degree of regularity along the polymer backbone.[18] Because vibronic peaks are not observed in PEDOT, we infer that PProDOT and PProDOT-Me_2 have a higher degree of regularity along their backbones than PEDOT. The bipolaronic peaks are also sharper in doped PProDOT and PProDOT-Me_2 than in doped PEDOT, consistent with this conclusion.

Isobestic points are evident in Fig. 8: PEDOT at 14 200 cm^{-1}, PProDOT at 15 600 cm^{-1}, and PProDOT-Me_2 at 15 000 cm^{-1}. The isobestic point occurs where the absorbance is independent of the doping level of the polymers.[19]

B. Doping-induced infrared active vibrational modes

Within the polaron or bipolaron picture of doped conjugated polymers, one expects a strong modification of the local structure around the additional electrons or holes introduced by doping. In turn, this can cause drastic changes in the vibrational properties of the polymer. These new infrared-active vibrational (IRAV) modes[20,21] are a common feature of doped conjugated polymers and have a number of remarkable features. Studies[22,23] of polyacetylene showed that the doping-induced infrared modes have oscillator strengths enhanced by $\approx 10^3$ compared to ordinary infrared-active phonons. Such a large enhancement is explained as arising from coupling of the new vibration modes (induced by doping) to the electronic oscillator strength of the polyacetylene chain. Another study[24] emphasized the generality of these results; the same modes were observed for different dopants (iodine, AsF_5, and Na). The observed generality suggests that the intense infrared absorption modes are intrinsic features of the doped polymers. Another theoretical study of the degenerate ground-state polymer polyacetylene[25] showed that the dominant motions associated with the IRAV of the soliton involve an antisymmetric contraction of the single (or double) bonds on the one side of the soliton center and expansion on the other, thus driving charge back and forth across the soliton center. It was also pointed out that the expected strengths of the IRAV of a soliton are large enough to be observable at very dilute doping. Although studied in less detail, evidence for IRAV effects have also been reported in nondegenerate ground-state polymers.[26–29]

The contribution to the absorption coefficient of both ordinary and doping-induced phonons is shown in Fig. 9 for the three polymers studied here. These curves are the difference between the absorption coefficients with and without the vibrational modes in the model Drude-Lorentz dielectric function. (In other words, we compute the absorption coefficient using the model and all of the parameters in Tables I–III, compute the absorption coefficient with the oscillator

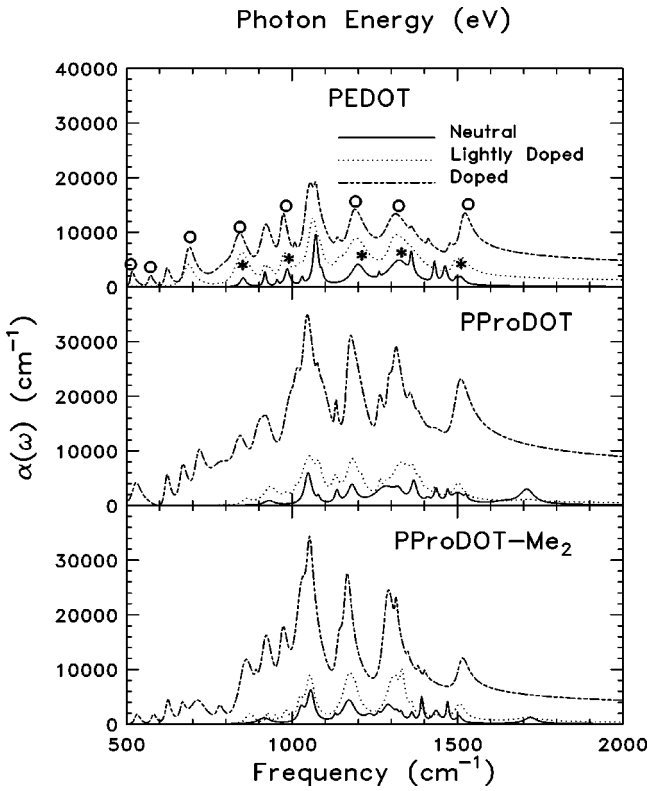

FIG. 9. Infrared-active vibration modes in PEDOT, PProDOT, and PProDOT-Me_2.

strengths of all the phonon modes set to zero, and then take the difference between these two curves.)

In situ IRAV and Raman spectra of PEDOT have been studied by several groups.[29–31] Comparing our absorption coefficients for neutral PEDOT with the reported absorbance of neutral PEDOT (Ref. 29) we find that our ''neutral state'' is not totally neutralized; five peaks from the doped segments, which we indicate with asterisks in Fig. 9, occur in these spectra. This conclusion is consistent with the electronic absorption (see the neutral state in Fig. 7 or Fig. 8) where residual absorption occurs in the 2000–4000 cm^{-1} range, below the π-π^* transition. Generally, the sharper vibrational peaks are due to the neutral polymer; these peaks do not grow with increased doping. The peaks that clearly do increase in strength with increasing doping in PEDOT are indicated with circles in Fig. 9. Moreover, when we compare the absorption coefficient of doped PEDOT with Raman-scattering data[30] for doped PEDOT we find that these peaks correspond to the Raman peaks of the neutral PEDOT. Doping causes Raman active modes to become infrared active, on account of a loss of translational symmetry induced by the doping process.

Sharp peaks in the neutral absorption coefficient correspond to characteristic vibrational modes for the pristine polymer. These peaks do not grow in the doped state, allowing us to identify neutral absorption peaks for PProDOT and PProDOT-Me_2. The peaks due to the neutral state are as follows: at 1047, 1135, 1367, 1410, 1435, 1470, and 1706 cm^{-1} for PProDOT and at 1027, 1362, 1395, 1435, 1470, and 1720 cm^{-1} for PProDOT-Me_2. (In all three materials the ClO_4^- absorption peak at 623 cm^{-1} is evident in the doped phase, because ClO_4^- ions were the dopant species.)

V. CONCLUSIONS

In summary, we have studied the optical properties of three nondegenerate ground-state conjugated polymers (PEDOT, PProDOT, and PProDOT-Me_2) in their neutral, lightly-doped, and fully doped states. We observed definite changes in the electronic spectra of these polymers, with the π-π^* transition, which occurs in the visible region in these materials, becoming bleached with doping, and disappearing completely in the fully doped state. This change with doping is the basis of the strong visible electrochromism observed in these polymers. At the same time, infrared absorption bands appear, interpreted within a picture of the doped carriers residing in polaron states in the lightly doped polymer and as bipolarons in the fully doped state. Evidence for strong electron-molecular vibration interactions were observed in the infrared region. Finally, all three systems had significant low-frequency conductivity when doped, with ClO_4^--doped PProDOT having the highest midinfrared (and estimated dc) conductivity, 390 S/cm.

ACKNOWLEDGMENTS

We gratefully acknowledge funding from the ARO/MURI program (Grant No. DAAD19-99-1-0316) and the AFOSR (Grant No. F49620-00-1-0047).

[1] C.K. Chiang, C.R. Fincher, Y.W. Park, A.J. Heeger, H. Shirakawa, E.J. Louis, S.C. Gau, and A.G. MacDiarmid, Phys. Rev. Lett. **39**, 1098 (1977).
[2] A.J. Heeger, S. Kivelson, J.R. Schrieffer, and W.P. Su, Rev. Mod. Phys. **60**, 781 (1988).
[3] K. Fesser, A.R. Bishop, and D.K. Campbell, Phys. Rev. B **27**, 4804 (1982).
[4] J.L. Brédas, R.R. Chance, and R. Silbey, Phys. Rev. B **26**, 5843 (1982).
[5] J.L. Brédas, B. Thémans, J.G. Fripiat, J.M. André, and R.R. Chance, Phys. Rev. B **29**, 6761 (1984).
[6] Y. Furukawa, J. Phys. Chem. **100**, 15 644 (1996).
[7] W.R. Salaneck, R.H. Friend, and J.L. Brédas, Phys. Rep. **319**, 231 (1999).
[8] H.W. Heuer, R. Wehrmann, and S. Kirchmeyer, Adv. Funct. Mater. **12**, 89 (2002).
[9] S.A. Sapp, G.A. Sotzing, and J.R. Reynolds, Chem. Mater. **10**, 2101 (1998).
[10] I. Schwendeman, J. Hwang, D.M. Welsh, D.B. Tanner, and J.R. Reynolds, Adv. Mater. **13**, 634 (2001).
[11] A. Kumar, D.M. Welsh, M.C. Morvant, F. Piroux, K.A. Abboud, and J.R. Reynolds, Chem. Mater. **10**, 896 (1998).

[12] D.M. Welsh, A. Kumar, E.W. Meijer, and J.R. Reynolds, Adv. Mater. **11**, 1379 (1999).
[13] G. Heywang and F. Jonas, Adv. Mater. **4**, 116 (1992).
[14] B. Sankaran and J.R. Reynolds, Macromolecules **30**, 2582 (1997).
[15] O.S. Heavens, *Optical Properties of Thin Solid Films* (Dover, New York, 1965).
[16] Frederick Wooten, *Optical Properties of Solids* (Academic, New York, 1972).
[17] P.R. Bevington, *Data Reduction and Error Analysis for the Physical Sciences* (McGraw-Hill, New York, 1969).
[18] S.D.D.V. Rughooputh, A.J. Heeger, and F. Wudl, J. Polym. Sci. A **25**, 1071 (1987).
[19] A. Feldblum, J.H. Kaufman, S. Etemad, A.J. Heeger, T.-C. Chung, and A.G. MacDiarmid, Phys. Rev. B **26**, 815 (1982).
[20] M.J. Rice, Phys. Rev. Lett. **37**, 36 (1976).
[21] B. Horovitz, Solid State Commun. **41**, 729 (1982).
[22] S. Etemad, A. Prón, A.J. Heeger, A.G. MacDiarmid, E.J. Mele, and M.J. Rice, Phys. Rev. B **23**, 5137 (1981).
[23] E. Ehrenfreund, Z. Vardeny, O. Brafman, and B. Horovitz, Phys. Rev. B **36**, 1535 (1987).
[24] C.R. Fincher, Jr., M. Ozaki, A.J. Heeger, and A.G. MacDiarmid, Phys. Rev. B **19**, 4140 (1979).
[25] E.J. Mele and M.J. Rice, Phys. Rev. Lett. **45**, 926 (1980).
[26] R.P. McCall, J.M. Ginder, M.G. Roe, G.E. Asturias, E.M. Scherr, A.G. MacDiarmid, and A.J. Epstein, Phys. Rev. B **39**, 10 174 (1989).
[27] K.F. Voss, C.M. Foster, L. Smilowitz, D. Mihailovic, S. Askari, G. Srdanov, Z. Ni, S. Shi, A.J. Heeger, and F. Wudl, Phys. Rev. B **43**, 5109 (1991).
[28] L. Smilowitz, N.S. Sariciftci, R. Wu, C. Gettinger, A.J. Heeger, and F. Wudl, Phys. Rev. B **47**, 13 835 (1993).
[29] C. Kvarnström, H. Neugebauer, A. Ivaska, and N.S. Sariciftci, J. Mol. Struct. **521**, 271 (2000).
[30] M. Lapkowski and A. Prón, Synth. Met. **110**, 79 (2000).
[31] S. Garreau, G. Louarn, J.P. Buisson, G. Froyer, and S. Lefrant, Macromolecules **32**, 6807 (1999).